Title
Interaction of CK1δ with γTuSC ensures proper microtubule assembly and spindle positioning

Journal
Molecular Biology of the Cell, 26(13)

ISSN
1059-1524

Authors
Peng, Yutian
Moritz, Michelle
Han, Xuemei
et al.

Publication Date
2015-07-01

DOI
10.1091/mbc.e14-12-1627

Peer reviewed

Interaction of CK1δ with γTuSC ensures proper microtubule assembly and spindle positioning

Yutian Peng[a], Michelle Moritz[b], Xuemei Han[c], Thomas H. Giddings[d], Andrew Lyon[b], Justin Kollman[b,*], Mark Winey[d], John Yates, III[c], David A. Agard[b], David G. Drubin[a], and Georjana Barnes[a]

[a]Department of Molecular and Cell Biology, University of California, Berkeley, Berkeley, CA 94720; [b]Department of Biochemistry and Biophysics, Howard Hughes Medical Institute, University of California, San Francisco, San Francisco, CA 94158; [c]Department of Chemical Physiology, Scripps Research Institute, La Jolla, CA 92037; [d]Department of Molecular, Cellular, and Developmental Biology, University of Colorado, Boulder, Boulder, CO 80309

ABSTRACT **Casein kinase 1δ (CK1δ) family members associate with microtubule-organizing centers (MTOCs) from yeast to humans, but their mitotic roles and targets have yet to be identified. We show here that budding yeast CK1δ, Hrr25, is a γ-tubulin small complex (γTuSC) binding factor. Moreover, Hrr25's association with γTuSC depends on its kinase activity and its noncatalytic central domain. Loss of Hrr25 kinase activity resulted in assembly of unusually long cytoplasmic microtubules and defects in spindle positioning, consistent with roles in regulation of γTuSC-mediated microtubule nucleation and the Kar9 spindle-positioning pathway, respectively. Hrr25 directly phosphorylated γTuSC proteins in vivo and in vitro, and this phosphorylation promoted γTuSC integrity and activity. Because CK1δ and γTuSC are highly conserved and present at MTOCs in diverse eukaryotes, similar regulatory mechanisms are expected to apply generally in eukaryotes.**

Monitoring Editor
Kerry S. Bloom
University of North Carolina

Received: Dec 18, 2014
Revised: May 4, 2015
Accepted: May 4, 2015

INTRODUCTION

The microtubule cytoskeleton is a highly dynamic structure that plays a pivotal role in a variety of cellular processes, including cell division, organelle positioning, motility, and intracellular transport. Microtubule dynamics are tightly controlled by a variety of mechanisms, of which microtubule nucleation provides control over global organization of the network and the timing of assembly.

Microtubules are nucleated by a γ-tubulin ring complex (γTuRC) in all eukaryotes. Two molecules of γ-tubulin and two molecules of the γ-tubulin complex proteins (GCPs) assemble into the γ-tubulin small complex (γTuSC), the basic subunit of the γTuRC. In most eukaryotes, there are five distantly related GCPs: GCP2–6, which share a common core structure (Kollman *et al.*, 2011; Remy *et al.*, 2013). Furthermore, additional proteins that do not exhibit these conserved GCP motifs, such as NEDD1 (GCP-WD) and Spc110, promote assembly and localization of the γTuRC to the centrosome and spindle pole, processes crucial for activation of γTuRC-mediated microtubule nucleation (Kollman *et al.*, 2011; Remy *et al.*, 2013). γTuRC is targeted primarily to three cellular structures (Teixido-Travesa *et al.*, 2012). At centrosomes, γTuRC nucleates microtubules that form the mitotic spindle or interphase microtubule array. γTuRC is also targeted to the Golgi apparatus, where microtubules help to maintain overall organization of the Golgi stacks and their location in the cell. Finally, during mitosis, γTuRC can be anchored to spindle microtubules laterally via a multiprotein complex termed augmin (Goshima *et al.*, 2008). Augmin complexes allow microtubules to nucleate from existing ones; this activity increases microtubule density within the spindle and influences microtubule dynamics.

Budding yeast contain only two GCPs: Spc97 (yeast GCP2) and Spc98 (yeast GCP3). Purified yeast γTuSC forms a Y-shaped structure with one γ-tubulin at the top of each lobe, interacting with Spc97 or Spc98 (Kollman *et al.*, 2008). Yeast γTuSC is anchored to the cytoplasmic and nuclear side of spindle pole bodies (SPBs; the yeast equivalent of centrosomes) by Spc72 and Spc110, respectively (Knop and Schiebel, 1997, 1998). The N-terminal domain of Spc110 promotes the oligomerization of yeast γTuSC into a ring structure or extended helical filaments in vitro, with 6½ γTuSCs or 13 γ-tubulins per turn (Kollman *et al.*, 2010). The fact that 13 γ-tubulins per turn matches the in vivo microtubule protofilament number

This article was published online ahead of print in MBoC in Press (http://www.molbiolcell.org/cgi/doi/10.1091/mbc.E14-12-1627) on May 13, 2015.

*Present address: Department of Biochemistry, School of Medicine, University of Washington, Seattle, WA 98195.

Address correspondence to: Georjana Barnes (gbarnes@berkeley.edu), David Drubin (drubin@berkeley.edu).

Abbreviations used: γTuRC, γ-tubulin ring complex; γTuSC, γ-tubulin small complex.

argues for a model in which γTuSC acts as a template for microtubule assembly, with γ-tubulin forming longitudinal interactions with α/β-tubulin. However, the arrangement of γ-tubulins in the γTuSC-Spc110 ring does not perfectly match the microtubule protofilament symmetry (Kollman *et al.*, 2010). Moreover, the γTuSC-Spc110 ring has a much lower nucleation activity than γTuRC (Kollman *et al.*, 2010), suggesting that γ-tubulin must undergo rearrangement to be fully activated, likely through protein–protein interaction and/or posttranslational modifications such as phosphorylation (Kollman *et al.*, 2011).

Although γTuRC components are reported to be phosphoproteins and a number of kinases involved in γTuRC function have been identified, how phosphorylation directly affects nucleation activity of γTuSC has only begun to be examined. It is known that in human cells, γ-tubulin is phosphorylated at Ser-131 by SADB kinase, which regulates centrosome duplication (Alvarado-Kristensson *et al.*, 2009). Similarly, GCP6 phosphorylation by Polo-like kinase 4 (Plk4) is also critical for centrosome duplication (Bahtz *et al.*, 2012). GCP5 binds to glycogen synthase kinase-3β (GSK-3β), and inhibition of GSK-3β disrupts targeting of γTuSC to centrosomes (Izumi *et al.*, 2008). Furthermore, targeting of γTuSC to centrosomes is regulated by phosphorylation of the non-GCP protein NEDD1 by a variety of kinases (Luders *et al.*, 2006; Haren *et al.*, 2009; Zhang *et al.*, 2009; Sdelci *et al.*, 2012). Recently human kinase NME7 was implicated in promoting microtubule nucleation by the γTuRC (Liu *et al.*, 2014).

In budding yeast, all components of γTuSC and Spc110 are phosphorylated in a cell cycle–dependent manner (Friedman *et al.*, 1996, 2001; Stirling and Stark, 1996; Pereira *et al.*, 1998; Keck *et al.*, 2011; Lin *et al.*, 2011, 2014). Cdk1 phosphorylates Tub4 (yeast γ-tubulin) at Ser-360, a Cdk1 consensus site that is conserved from yeast to mammals. Mutating Ser-360 to Ala does not cause a growth defect, whereas mutating it to Asp destabilizes Tub4 and arrests cells at metaphase (Keck *et al.*, 2011; Lin *et al.*, 2011). In addition, Tub4 is phosphorylated at highly conserved Tyr-445 by an unknown kinase. A Tyr445Phe mutant exhibits no growth defects. In contrast, a Tyr445Asp mutant shows a metaphase arrest at 34°C (Vogel *et al.*, 2001). Spc97 and Spc98 are also phosphorylated on multiple residues in vivo. Mutating a subset of Spc97 phosphorylation sites led to slow growth, whereas no mutants of Spc98 phosphorylation sites made to date exhibit obvious defects (Lin *et al.*, 2011). Recently Spc110 phosphorylation by Cdk1 and Mps1 was reported to promote γTuSC oligomerization and therefore activation of microtubule nucleation (Lin *et al.*, 2014).

The foregoing studies highlight the conclusion that localization and activity of γTuRC are tightly regulated by a complex set of protein kinases. Here we identified a novel kinase-binding partner of yeast γTuSC, Hrr25, the budding yeast homologue of human casein kinase 1δ (CK1δ). CK1δ, a member of the highly conserved CK1 family (Petronczki *et al.*, 2006), is involved in a wide variety of signaling pathways (Knippschild *et al.*, 2005a,b; Cheong and Virshup, 2011; Perez *et al.*, 2011). In mammalian cells, CK1δ is enriched at centrosomes in addition to the Golgi and mitotic spindle (Behrend *et al.*, 2000; Milne *et al.*, 2001; Andersen *et al.*, 2003; Greer and Rubin, 2011). Inhibition of CK1δ results in enlarged centrosome morphology and abnormal mitotic spindles in extravillous trophoblast hybrid cells (Stoter *et al.*, 2005). CK1δ localization at centrosomes is dependent on its own kinase activity (Milne *et al.*, 2001) and its noncatalytic C-terminus (Greer and Rubin, 2011). In neuronal TC-32 cells, removal of native CK1δ from centrosomes caused defects in neurite outgrowth, a process requiring proper centrosome-mediated microtubule dynamics (Greer and Rubin, 2011). However, whether CK1δ interacts with and/or phosphorylates γTuRC remains to be determined.

Similar to its varied localizations (centrosomes, spindle, and Golgi) in mammalian cells, CK1δ (Hrr25) is localized not only to SPBs in budding yeast, but also to the bud neck and endocytic sites (Kafadar *et al.*, 2003; Lusk *et al.*, 2007; Peng *et al.*, 2015). Like CK1δ, Hrr25 functions in a wide range of cellular processes (Hoekstra *et al.*, 1991; Murakami *et al.*, 1999; Schafer *et al.*, 2006; Ray *et al.*, 2008; Lord *et al.*, 2011). In this article, we investigate two critical and as-yet-unanswered questions: how Hrr25 is recruited to yeast microtubule-organizing centers (SPBs), and how it affects microtubule assembly.

RESULTS

Hrr25 is targeted to three distinct cellular structures by specific proteins/protein complexes

Hrr25–triple green fluorescent protein (3GFP) expressed from the endogenous *HRR25* locus localizes to three distinct cellular structures: endocytic patches at the plasma membrane (Peng *et al.*, 2015), the bud neck (Kafadar *et al.*, 2003; Peng *et al.*, 2015), and SPBs (Lusk *et al.*, 2007; Peng *et al.*, 2015; Figure 1B). Our previous work showed that Hrr25 recruitment to endocytic sites depends on Ede1, an Eps15 homologue in yeast (Peng *et al.*, 2015). To identify the proteins that might target Hrr25 to the bud neck and SPBs, we expressed a tandem affinity–tagged Hrr25 (Hrr25-TAP) from its endogenous genomic locus in yeast cells and analyzed the proteins that copurified with Hrr25 by mass spectrometry (Figure 1A and Supplemental Table S1). Using a previously established computational method (Michelot *et al.*, 2010), we identified proteins enriched in the Hrr25-TAP sample by comparing the mass spectrometry data with PeptideAtlas data (www.peptideatlas.org/). Consistent with previous observations, Ede1 (Peng *et al.*, 2015) and Mam1 (Petronczki *et al.*, 2006), a component of the monopolin complex, copurified with Hrr25, demonstrating that our conditions for Hrr25-TAP purification identify bona fide Hrr25-interacting proteins. Among the highly enriched copurified proteins, we found all three components of γTuSC: Tub4, Spc97, and Spc98. In addition, we detected Cyk3 and Hof1, two proteins that function in cytokinesis and interact with each other.

On the basis of the results of the mass spectrometry analysis, we next investigated how Hrr25-interacting proteins affect Hrr25 recruitment to the bud neck and SPBs. Deletion of *CYK3* alone did not affect Hrr25 localization to endocytic patches or SPBs (Figure 1B). Because endocytic patches are enriched at the bud neck, it was not possible to determine whether loss of Cyk3 affects Hrr25 localization at the cytokinesis site. We therefore created the double-deletion mutant *cyk3*Δ *ede1*Δ. We observed that Hrr25 is absent from the bud neck in *cyk3*Δ *ede1*Δ cells but not in *ede1*Δ cells (Figure 1B).

To test whether γTuSC recruits Hrr25 to SPBs, we first confirmed that Hrr25 localizes at SPBs and not at kinetochores, since these two structures are near each other during most of the cell cycle. We imaged Hrr25-3GFP together with either Mtw1–red fluorescent protein (RFP; kinetochore marker) or Spc42-mCherry (SPB marker) in an *ede1*Δ background. We found that, at metaphase/early anaphase, Hrr25 always colocalizes with Spc42 but not with Mtw1, which localizes internal to the SPBs in spindles (Figure 1C), confirming that Hrr25 resides at SPBs. We further demonstrated, by immuno–electron microscopy, that Hrr25 is located at SPBs (Figure 1D). Because Tub4, Spc97, and Spc98 are all essential for cell viability, we used an auxin-induced degradation (AID) system to specifically degrade each protein and determined whether the degradation of these proteins

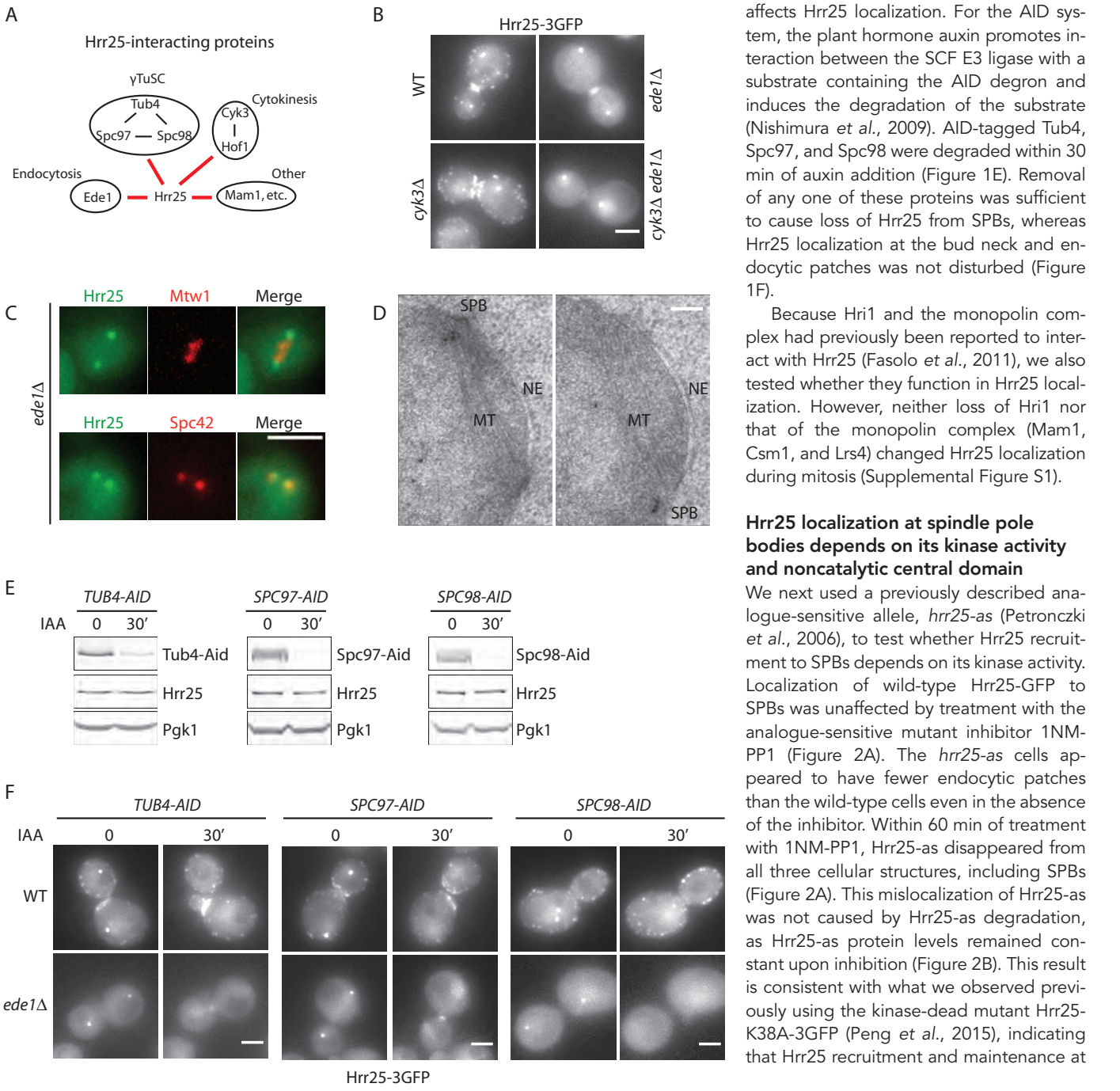

FIGURE 1: Hrr25 is targeted to three distinct cellular structures by three specific proteins/protein complexes. (A) Hrr25-TAP was purified, and the indicated Hrr25-associated proteins were identified by mass spectrometry. Red lines represent the interactions identified in this study, and black lines represent the interactions reported previously. A complete list of Hrr25-associated proteins is provided in Supplemental Table S4. (B) Maximum intensity *Z*-projection of Hrr25-3GFP in wild-type, *ede1*Δ, *cyk3*Δ, and *ede1*Δ *cyk3*Δ cells. Scale bar, 2 μm. (C) Maximum intensity *Z*-projections of Hrr25-3GFP with a kinetochore protein (Mtw1-RFP) or a SPB protein (Spc42-mCherry) in *ede1*Δ cells. Scale bar, 2 μm. (D) Immuno–electron micrograph (EM) of Hrr25-3GFP location. Two sections of the same cell are shown. Hrr25-3GFP location was identified by immunolabeling using a GFP antibody and a colloidal gold-conjugated secondary antibody. The immuno-EM labeling of nine cells expressing Hrr25-GFP was evaluated from two or three sections per cell that included one or both of the SPBs and part of the nucleus. Of 122 gold particles on the cells, 28 were on the inner plaque of the SPB, with only two particles on other parts of the SPB. There were 70 particles in the nucleus and 22 particles in the cytoplasm. All of this signal likely reports the location of Hrr25-GFP because the conditions and anti-GFP reagents used in this experiment give nearly no background signal on cells lacking GFP. Of importance, the high number of particles over the small area of the inner plaque clearly suggests that the SPB inner plaque is the major cellular location of Hrr25. MT, microtubules; NE, nuclear envelope; SPB, spindle pole body. Scale bar, 100 nm. (E, F) The indicated auxin-inducible degron (AID) cells were treated with 0.1 mM auxin for 30 min at 25°C. Cells were collected and subjected to immunoblotting (E) and imaging (F). Maximum intensity *Z*-projections of Hrr25-3GFP in wild-type or *ede1*Δ cells are shown. Scale bars, 2 μm.

affects Hrr25 localization. For the AID system, the plant hormone auxin promotes interaction between the SCF E3 ligase with a substrate containing the AID degron and induces the degradation of the substrate (Nishimura *et al.*, 2009). AID-tagged Tub4, Spc97, and Spc98 were degraded within 30 min of auxin addition (Figure 1E). Removal of any one of these proteins was sufficient to cause loss of Hrr25 from SPBs, whereas Hrr25 localization at the bud neck and endocytic patches was not disturbed (Figure 1F).

Because Hri1 and the monopolin complex had previously been reported to interact with Hrr25 (Fasolo *et al.*, 2011), we also tested whether they function in Hrr25 localization. However, neither loss of Hri1 nor that of the monopolin complex (Mam1, Csm1, and Lrs4) changed Hrr25 localization during mitosis (Supplemental Figure S1).

Hrr25 localization at spindle pole bodies depends on its kinase activity and noncatalytic central domain

We next used a previously described analogue-sensitive allele, *hrr25-as* (Petronczki *et al.*, 2006), to test whether Hrr25 recruitment to SPBs depends on its kinase activity. Localization of wild-type Hrr25-GFP to SPBs was unaffected by treatment with the analogue-sensitive mutant inhibitor 1NM-PP1 (Figure 2A). The *hrr25-as* cells appeared to have fewer endocytic patches than the wild-type cells even in the absence of the inhibitor. Within 60 min of treatment with 1NM-PP1, Hrr25-as disappeared from all three cellular structures, including SPBs (Figure 2A). This mislocalization of Hrr25-as was not caused by Hrr25-as degradation, as Hrr25-as protein levels remained constant upon inhibition (Figure 2B). This result is consistent with what we observed previously using the kinase-dead mutant Hrr25-K38A-3GFP (Peng *et al.*, 2015), indicating that Hrr25 recruitment and maintenance at

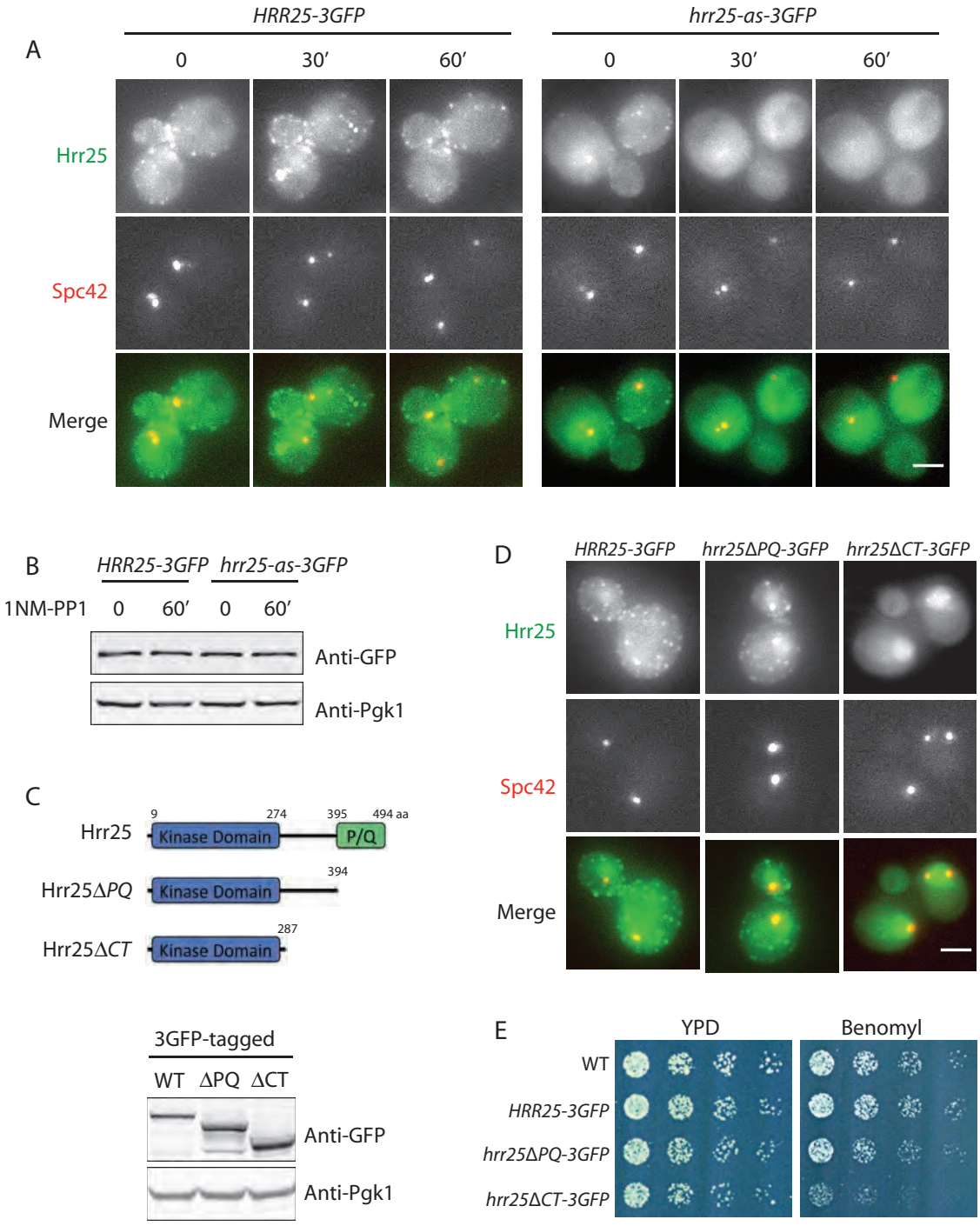

FIGURE 2: Hrr25 localization at spindle pole bodies depends on its kinase activity and noncatalytic C-terminus. (A) Cells expressing Hrr25-3GFP and Spc42-mCherry or Hrr25-as-3GFP and Spc42-mCherry from their respective endogenous genomic loci were treated with 35 μM 1NM-PP1 (or an equal volume of dimethyl sulfoxide) at 25°C. Maximum intensity *Z*-projections of representative cells are shown. Scale bar, 2 μm. (B) *HRR25-3GFP* and *hrr25-as-3GFP* cells were treated as described. Whole-cell protein extracts were analyzed by immunoblotting. (C) Whole-cell protein extracts from cells expressing *HRR25-3GFP*, *hrr25ΔPQ-3GFP*, and *hrr25ΔCT-3GFP* were analyzed by immunoblotting. (D) Maximum intensity *Z*-projections of Hrr25-3GFP, Hrr25ΔPQ-3GFP, and Hrr25ΔCT-3GFP with Spc42-mCherry. Representative cells are shown. Scale bar, 2 μm. (E) Equal numbers of indicated cells were grown on YPD or YPD containing benomyl (10 μg/ml) plates at 25°C.

SPBs, the bud neck, and endocytic patches depend on its kinase activity.

Hrr25 is composed of a highly conserved kinase domain (amino acids [aa] 9–274) at its N-terminus and a proline/glutamine (P/Q)–rich domain (aa 395–494) at its C-terminus (Figure 2C). The latter domain is unique to the yeast protein. The Hrr25 central domain (aa 275–394) has 21% amino acid sequence identity to the centrosomal localization signal found at the noncatalytic C-terminus of human

CK1δ (Greer and Rubin, 2011). We therefore tested whether Hrr25's central domain is required for its recruitment to SPBs, by expressing truncation mutants in yeast (Figure 2C). Deletion of the P/Q-rich domain (*hrr25ΔPQ*) did not affect Hrr25 localization. In contrast, further deletion of the central domain (*hrr25ΔCT*) abolished endocytic patch localization of the kinase. Moreover, Hrr25ΔCT was no longer enriched at SPBs and became diffuse throughout the nucleus (Figure 2D). The latter mutant also caused increased sensitivity to the microtubule-depolymerizing drug benomyl, providing evidence that recruitment of Hrr25 to the SPB is important for microtubule function (Figure 2E).

Loss of Hrr25 kinase activity results in long cytoplasmic microtubules at G1 phase

To investigate Hrr25's function at SPBs, we first tested *hrr25* mutants for sensitivity to benomyl. Intriguingly, both *HRR25-AID* and *hrr25-as* conferred benomyl resistance to otherwise wild-type cells (Figure 3, A and B), suggesting that microtubule assembly might be enhanced in these *hrr25* mutants. Various mutants with enhanced microtubule assembly properties, including *tub4* mutants, confer benomyl resistance (Vogel and Snyder, 2000; Gombos *et al.*, 2013). In addition, *tub4* mutants also exhibit unusually long cytoplasmic microtubules (Marschall *et al.*, 1996). Similarly, in *hrr25-as* cells in the presence of 1NM-PP1, we observed long cytoplasmic microtubules in G1-phase cells (Figure 3C). Once SPB duplication was complete, Hrr25 inhibition did not result in any obvious defects (unpublished data). We next sought to quantify the differences in microtubule length in G1-phase cells. To do this, we synchronized *hrr25-as* cells and isogenic wild-type *HRR25* cells with α-factor and released the cells into medium containing 1NM-PP1. At 60 min after the release, the average length of cytoplasmic microtubules in *HRR25* cells was 2.4 μm, whereas it was 8.3 μm in *hrr25-as* cells (Figure 3D).

Hrr25 functions in the Kar9 spindle-positioning pathway

Proper control of cytoplasmic microtubule assembly is essential for spindle positioning during early anaphase. In budding yeast, two functionally redundant pathways control spindle positioning—the Kar9 pathway and the dynein pathway (Li *et al.*, 1993; Miller *et al.*, 1999). Compromising either pathway alone causes little effect, whereas loss of both pathways leads to spindle misorientation and consequently failure of proper chromosome segregation. A global

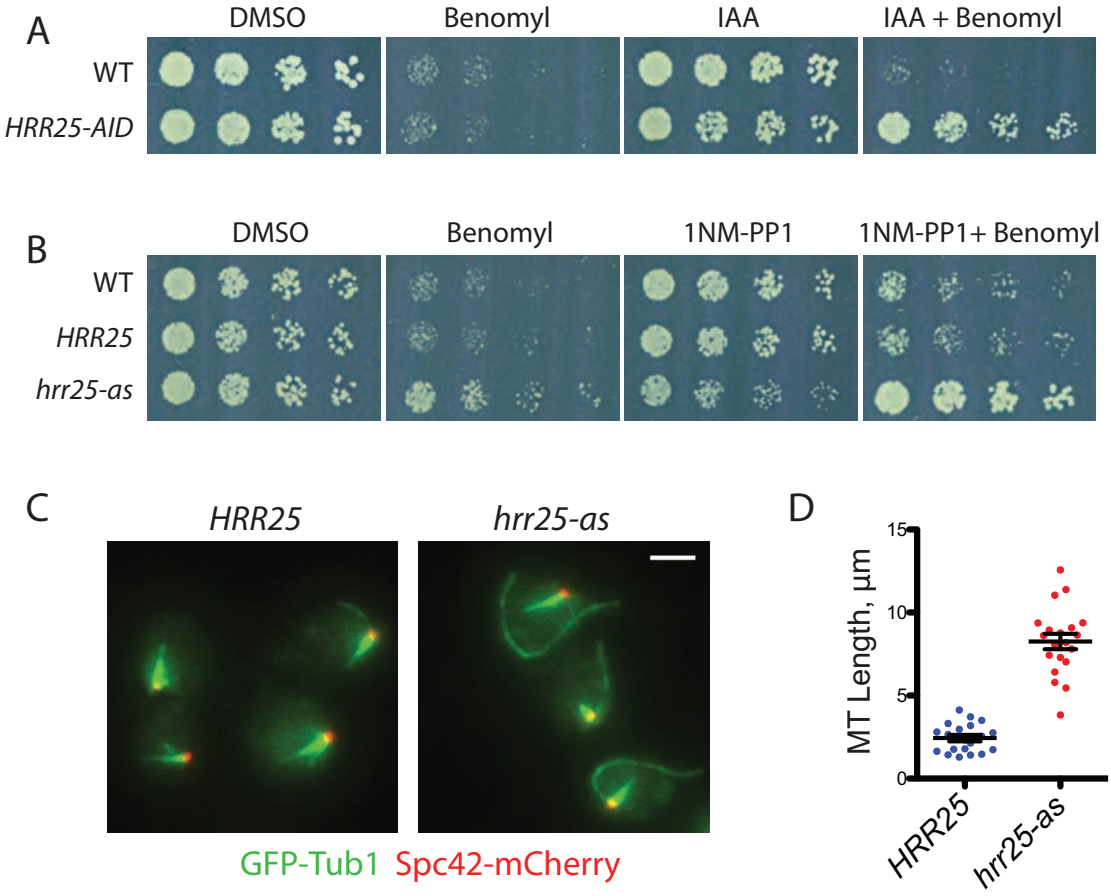

FIGURE 3: Loss of Hrr25 kinase activity results in long cytoplasmic microtubules in G1 phase. (A) Equal numbers of wild-type and *HRR25-AID* cells were grown on the indicated YPD supplemented plates at 25°C. Benomyl, 15 μg/ml; auxin, 0.1 mM. (B) Equal numbers of wild-type, *HRR25*, and *hrr25-as* cells were grown on the indicated YPD supplemented plates at 25°C. Benomyl, 15 μg/ml; 1NM-PP1, 200 nM. (C) *HRR25* and *hrr25-as* cells expressing GFP-Tub1 and Spc42-mCherry were synchronized with α-factor and then released into medium containing 35 μM 1NM-PP1 at 25°C. The cells were imaged at 1 h after release. Maximum intensity *Z*-projections are presented. Scale bar, 2 μm. (D) The lengths of cytoplasmic microtubules in *HRR25* and *hrr25-as* cells were measured. Averages (black bars) from 20 cells are presented for each strain. Error bars represent SEM.

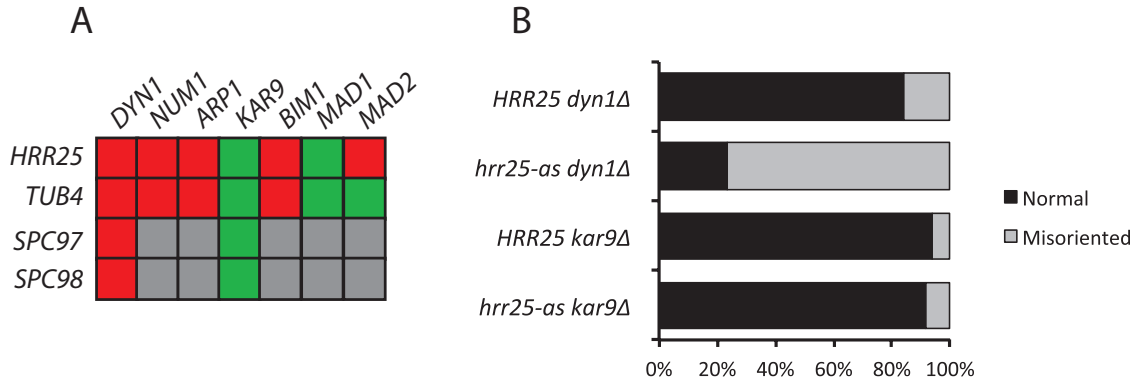

FIGURE 4: Hrr25 functions in the Kar9 spindle-positioning pathway. (A) Genetic interactions of *HRR25*, *TUB4*, *SPC97*, and *SPC98* with spindle-positioning pathways. Red represents negative genetic interaction, green represents no genetic interaction, and gray represents an interaction not tested. (B) The indicated cells expressing GFP-Tub1 were arrested in 0.1 M hydroxyurea and released into medium containing 35 μM 1NM-PP1 at 25°C. Spindle-positioning defects (both SPBs are present in the mother cells at the late anaphase) were scored at 2 h after release and are presented as percentage of total cells with normal spindle positioning. n = 216, 194, 373, and 367 cells for *HRR25 dyn1*Δ, *hrr25-as dyn1*Δ, *HRR25 kar9*Δ, and *hrr25-as kar9*Δ, respectively.

genetic interaction study revealed negative genetic interactions between *HRR25* and components of the dynein pathway, including *DYN1*, *NUM1*, and *ARP1* (Costanzo *et al.*, 2010). Consistently, we found that *hrr25-as* exhibits negative genetic interactions with *dyn1*Δ and *num1*Δ but not with *kar9*Δ (Supplemental Figure S2A). Of interest, *HRR25* genetic interactions resemble previously reported *TUB4* genetic interactions (Cuschieri *et al.*, 2006; Figure 4A), predictive of a common function. In addition to *dyn1*Δ and *num1*Δ, *hrr25-as* and *tub4* mutants had a negative genetic interaction with *bim1*Δ (Supplemental Figure S2A; Cuschieri *et al.*, 2006), presumably due to Bim1's central role at the plus ends of microtubules and the fact that it influences many aspects of microtubule dynamics. We further examined the genetic interactions of *SPC97-AID* or *spc98-1* with *dyn1*Δ or *kar9*Δ. Like *TUB4-AID*, both *SPC97-AID* and *spc98-1* had negative genetic interactions with *dyn1*Δ, but not with *kar9*Δ (Figure 4A and Supplemental Figure S2, B–D).

We next directly tested the role of Hrr25 in spindle positioning. Wild-type or *hrr25-as* cells were synchronized with hydroxyurea and released into medium containing the inhibitor 1NM-PP1. At 2 h after release, mitotic spindles in wild-type cells elongated, with one spindle pole in the mother cell and the other in the daughter cell, whereas in spindle-positioning mutants, both spindle poles resided in the mother cell. Inhibition of Hrr25 kinase activity in the *dyn1*Δ genetic background (*hrr25-as dyn1*Δ) resulted in a severe defect in spindle positioning. Only 23.2% of *hrr25-as dyn1*Δ cells, compared with 84.3% *HRR25 dyn1*Δ cells, exhibited proper spindle positioning. In contrast, inhibition of Hrr25 kinase activity in the *kar9*Δ genetic background had little effect, as 91.6% *hrr25-as kar9*Δ cells and 94.1% *HRR25 kar9*Δ cells showed normal spindle positioning (Figure 4B). Taken together, the foregoing analyses indicate that *hrr25* mutants exacerbate spindle-positioning defects of mutants in the dynein but not the Kar9 pathway. We therefore conclude that Hrr25 kinase activity is required for the Kar9 pathway.

Hrr25 phosphorylates γTuSC in vivo and in vitro

To investigate how Hrr25 might regulate γTuSC, we first examined whether loss of Hrr25 changes γTuSC localization. To eliminate possible variation caused by inconsistent imaging conditions, we mixed one strain expressing wild-type Hrr25 and mCherry-Tub1 with another expressing Hrr25-Aid but not mCherry-Tub1, so that the wild-type and Hrr25-Aid cells could be distinguished by the presence of mCherry. We then treated the mixed cells with auxin for 3 h. In the absence of Hrr25, all three components of γTuSC continue to localize at SPBs (Figure 5, A–C). In addition, levels of Tub4-GFP, Spc97-GFP, and GFP-Spc98 did not change when Hrr25-Aid was degraded (Figure 5, D–F). Of interest, we observed that GFP-Spc98 exhibited two electrophoretic protein forms when Hrr25 was present but that the slow-migrating form collapses to the fast-migrating form when Hrr25 is degraded (Figure 5F). Previously it was reported that a slow-migrating Spc98 species is phosphorylated Spc98 (Pereira *et al.*, 1998). The foregoing results indicate that loss of Hrr25 leads to a decrease in Spc98 phosphorylation. Furthermore, we found that integrity of γTuSC is required for the complex to localize at SPBs. Degradation of one component of γTuSC resulted in delocalization of the other two components from the SPBs (Supplemental Figure S3). Of note, when Spc98 delocalized from SPBs, it became dephosphorylated, presumably because it was no longer in proximity to Hrr25 (Supplemental Figure S3, A and B).

We next tested whether Hrr25 directly phosphorylates γTuSC in vitro. Full-length Hrr25, Hrr25ΔPQ, and their corresponding kinase-dead mutants were overexpressed in yeast and purified by affinity chromatography. Removal of the P/Q-rich domain of Hrr25 enhanced protein solubility. We found that Hrr25, but not the kinase-dead mutant Hrr25-K38A, phosphorylated all three γTuSC components. Of note, Spc98 phosphorylation resulted in an apparent upward electrophoretic shift (Figure 5G). In addition, we observed that Hrr25ΔPQ had similar kinase activity to full-length Hrr25 (Figure 5H), consistent with what we observed in vivo. That is, deletion of the P/Q–rich domain did not cause any detectable defect in growth (Peng *et al.*, 2015) or Hrr25 mislocalization (Figure 2D).

Hrr25 stimulates γTuSC-mediated microtubule nucleation in vitro

We next asked whether Hrr25 directly regulates γTuSC-mediated microtubule nucleation in vitro. To this end, we first tested whether

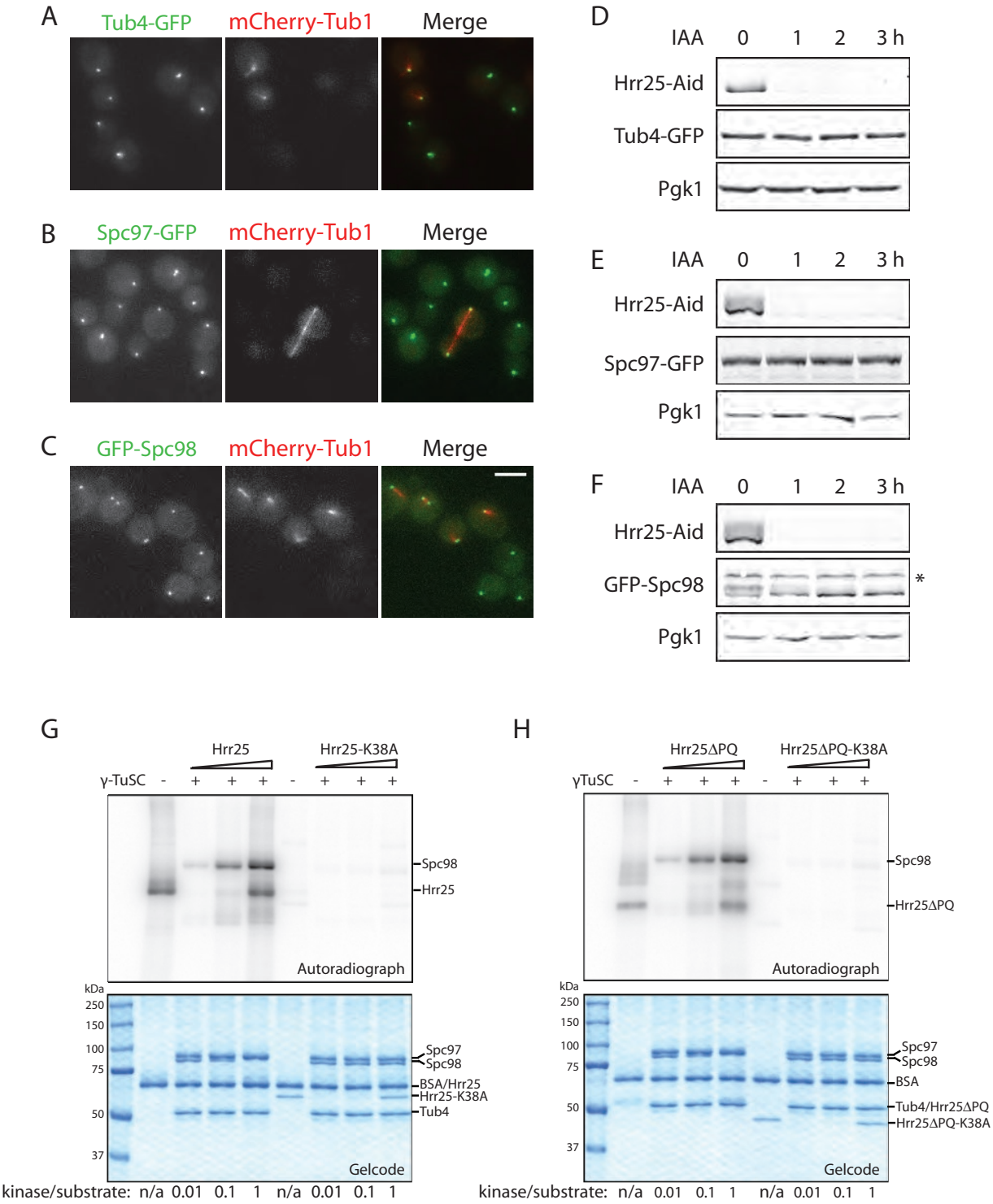

FIGURE 5: Hrr25 phosphorylation of γTuSC in vivo and in vitro. (A) Cells expressing Hrr25-Aid and Tub4-GFP were mixed with cells expressing Tub4-GFP and mCherry-Tub1. The mixed cells were then treated with 1 mM auxin for 3 h and imaged. Maximum intensity *Z*-projections of representative cells are presented. (B) Cells expressing Hrr25-Aid and Spc97-GFP were mixed with cells expressing Spc97-GFP and mCherry-Tub1. The mixed cells were treated and imaged as in A. (C) Cells expressing Hrr25-Aid and GFP-Spc98 were mixed with cells expressing GFP-Spc98 and mCherry-Tub1. The mixed cells were treated and imaged as in A. Scale bar, 2 μm. (D) Cells expressing Hrr25-Aid and Tub4-GFP were treated with 1 mM auxin at 25°C and collected at the indicated time points for immunoblotting. (E) Cells expressing Hrr25-Aid and Spc97-GFP were treated and subjected to immunoblotting as in D. (F) Cells expressing Hrr25-Aid and GFP-Spc98 were treated and subjected to immunoblotting as in D. *Nonspecific band. (G) γTuSC (2.5 pmol) was incubated with 0, 0.025, 0.25, or 2.5 pmol of Hrr25 or Hrr25-K38A in the presence of [γ^{32}P]ATP at room temperature for 30 min. Phosphorylation was analyzed by autoradiography after SDS–PAGE. (H) The same in vitro kinase assays described in G were performed using Hrr25ΔPQ or Hrr25ΔPQ-K38A.

Hrr25 binds directly to γTuSC. Purified Hrr25ΔPQ or kinase-dead mutant tagged with streptavidin (Strep) was incubated with pure γTuSC and then pulled down by Strep-Tactin beads. The binding was measured by monitoring the unbound γTuSC (Pollard, 2010). At conditions in which the molar ratio of kinase versus γTuSC was 1:1, the amount of unbound γTuSC was comparable to that of the control (no kinase). However, at the molar ratio of 8:1, K38AΔPQ was able to deplete γTuSC completely. In contrast, Hrr25 depleted γTuSC only partially, suggesting that the kinase mutant K38AΔPQ binds to γTuSC more tightly than wild-type kinase (Hrr25ΔPQ) in both the absence and presence of ATP (Figure 6A).

We next tested whether Hrr25 affects γTuSC nucleating activity. γTuSC-Spc110 at 100 nM was incubated with pig tubulin in the presence of Hrr25ΔPQ or K38AΔPQ. At a low nanomolar concentration of kinases (12.5 and 25 nM), we observed that Hrr25ΔPQ increased the number of microtubules assembled, whereas K38AΔPQ did not (Figure 6, B and C), supporting the notion that kinase activity of Hrr25 stimulates γTuSC-mediated microtubule-nucleating activity. As the kinase concentration increased (50 and 100 nM), addition of either Hrr25ΔPQ or K38AΔPQ resulted in similar increases in microtubule numbers (Figure 6, B and C). Given that K38AΔPQ binds to γTuSC with a higher affinity, we postulate that both Hrr25 phosphorylation of γTuSC and its binding to γTuSC contribute to promotion of nucleating activity.

Hrr25 phosphorylation of yeast γ-tubulin is required for γTuSC function in vivo

The foregoing results indicate that Hrr25 kinase activity stimulates γTuSC microtubule-nucleating activity in vitro. To test how Hrr25 kinase activity might affect γTuSC function in vivo, we first mapped phosphorylation sites of γTuSC. Hrr25- and Hrr25-K38A-treated γTuSCs were subjected to mass spectrometry analysis. Because γTuSC was expressed in Sf9 cells and posttranslationally modified in those cells before in vitro kinase assays were performed, we included nontreated γTuSC as a control. Because Hrr25 phosphorylates serines, threonines, and tyrosines (Hoekstra *et al.*, 1994), we included tyrosines in our mass spectrometry analysis. We identified 22 Hrr25-phosphorylation sites in Tub4, 14 in Spc97, and 14 in Spc98. Supporting the validity of our results, several of the Hrr25-phosphorylation sites we identified were predicted to be CK1δ sites based on their sequences, in which an acidic residue or phosphorylated serine/threonine/tyrosine resides at the –3 position (D/E-x-x-S/T or pS/T/Y-x-x-ST, where x indicates any amino acid; Supplemental Table S2).

We next examined where the Hrr25-phosphorylation sites are located in a modeled structure of the yeast γTuRC, based on the crystal structures of human GCP4 (Guillet *et al.*, 2011), human γ-tubulin (Aldaz *et al.*, 2005), and a cryo–electron microscopy structure of γTuRC (Kollman *et al.*, 2015). We found that several Tub4-phosphorylation sites are in regions potentially critical for Tub4 function (Figure 7A) and decided to focus on these for this study. Among these, S58 is in the H1-S2 loop, which interacts with the M-loop on a neighboring γ-tubulin during lateral interactions (γ-tubulin structure nomenclature is defined as described previously; Inclan and Nogales, 2001; Lowe *et al.*, 2001). S71 and S74 are predicted to be at the interface between γ-tubulin and α-tubulin and close to the GTP-binding pocket of γ-tubulin (T2-loop and H2). GTP binding to γ-tubulin was shown to promote interaction between γ-tubulin and α/β-tubulin and thereby activate microtubule nucleation (Gombos *et al.*, 2013). S208 is in helix 6, which has been proposed to undergo a conformational change that is important in microtubule assembly (Aldaz *et al.*, 2005). Finally, a short sequence stretch containing five phosphorylation sites (S277, Y279, S290, S291, Y292) resides in the M-loop at the interface between two adjacent γ-tubulins and is thus potentially important for γ-tubulin/γ-tubulin lateral interactions.

We mutated the aforementioned phosphorylation sites to Ala/Phe (nonphosphorylatable) or Asp/Glu (phosphomimicking). Because *TUB4* is an essential gene, we created the phosphomutants in the background of *TUB4-AID*. In the absence of auxin, all mutants were viable. However, in the presence of auxin, *tub4-2A*, *2D*, and *5AF* became lethal (Figure 7B). Of interest, in the presence of auxin, the lethality of *tub4-2A* and *tub4-2D* was suppressed by benomyl, whereas the lethality of *tub4-5AF* was not (Figure 7B), suggesting that these mutations affected Tub4 in a different manner.

We further examined γTuSC localization and microtubule dynamics in the phosphomutants. As described earlier, we established that γTuSC integrity is essential for its proper localization at SPBs (Supplemental Figure S3). Here we used GFP-Spc98 localization to monitor γTuSC integrity. In contrast to wild-type *TUB4* cells, after 1 h of auxin treatment in *tub4Δ* cells, microtubules became broken and faint, and GFP-Spc98 was no longer localized at SPBs (Figure 7C). In cells expressing *tub4-2A* or *tub4-2D* mutants, GFP-Spc98 was localized to SPBs, indicating that γTuSC is intact; however, these mutant cells arrested with short spindles and an abnormally large-budded, elongated cell shape (Figure 7C). The nonphosphorylatable mutants *tub4-5AF* exhibited phenotypes similar to *tub4Δ*. In contrast, cells containing the phosphomimicking mutants *tub4-5DE* appeared the same as wild-type cells. On the basis of these phenotypes, we suggest that phosphorylation at S71 and S74 by Hrr25 and possibly other mitotic regulators may be important for γTuSC nucleation activity, whereas phosphorylation at S277, Y279, S290, S291, and Y292 may be important for inter/intra-γTuSC interactions and γTuSC stability/integrity at SPBs.

DISCUSSION

In budding yeast, Cdk1, Mps1, and polo kinase Cdc5 are known to phosphorylate SPB proteins (Pereira *et al.*, 1998; Castillo *et al.*, 2002; Crasta *et al.*, 2008). Among these kinases, Cdk1 and Cdc5 are enriched at SPBs (Song *et al.*, 2000; Maekawa *et al.*, 2003). Here we identified Hrr25 as a novel SPB-associated kinase and demonstrated that localization of Hrr25 at SPBs specifically depends on γTuSC (Figure 1). Moreover, we showed that Hrr25 kinase activity is required for its localization at SPBs in vivo (Figure 2). However, our in vitro binding assays indicated that the kinase-dead mutant binds to γTuSC with a higher affinity than the wild-type kinase at a high molar ratio to γTuSC (Figure 6), which contradicts what we observed in vivo. These results suggest that there are additional levels of complexity in Hrr25 regulation that need to be investigated in future studies.

Our data showed that Hrr25 stimulates γTuSC-mediated microtubule nucleation at lower molar concentrations than the kinase-dead mutant of Hrr25. However, we observed Hrr25 and the kinase-dead mutant equally promote microtubule nucleation at closer to equimolar concentrations. One possible explanation is that both Hrr25 binding and γTuSC phosphorylation contribute to γTuSC-mediated nucleating activity. For example, binding may in itself elicit a conformational change in γTuSC that enhances its nucleating activity. Kinase-dead Hrr25 appeared to have a higher affinity for γTuSC in vitro, which might compensate for its lack of kinase activity. It will be important in the future to determine the in vivo molar ratio of Hrr25 to γTuSC and explore structurally the interaction between the kinase and nucleating complex to further understand how Hrr25 affects γTuSC assembly and function.

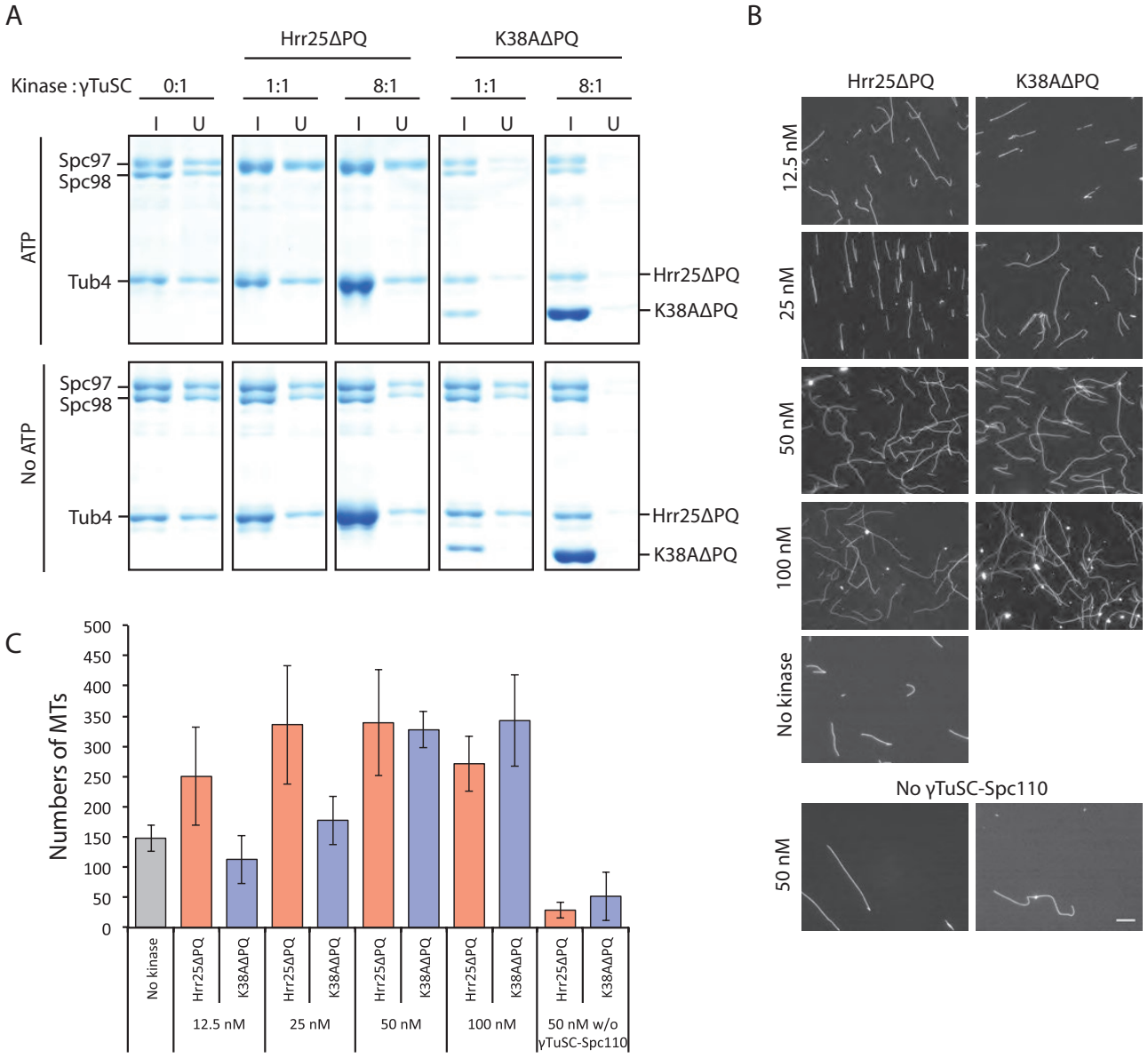

FIGURE 6: Hrr25 stimulates γTuSC-mediated microtubule assembly in vitro at low concentrations (25 and 12.5 nM), whereas both Hrr25 and Hrr25-K38A stimulate microtubule assembly at high concentrations (100 and 50 nM). (A) γTuSC (His-tagged) was mixed and incubated with Hrr25ΔPQ or K38AΔPQ (Strep-His-tagged) for 1 h at room temperature in the absence or presence of ATP and $MgCl_2$. Strep-Tactin magnetic beads were added to the protein mixtures and continued to incubate at room temperature for 1 h. The total input (I) and unbound proteins (U) were analyzed by SDS–PAGE and Gelcode blue staining. Kinase:γTuSC indicates the molar ratio of kinase vs. γTuSC. Note that Hrr25ΔPQ ran at the same molecular weight as Tub4. Spc98 demonstrated an upward electrophoretic shift in the presence but not in the absence of ATP. (B) Pig brain tubulin (16 μM) and γTuSC-Spc110$^{1\text{-}401}$ (100 nM γTuSC) were incubated at 30°C for 20 min with no kinase or with the indicated concentrations of Hrr25ΔPQ or K38AΔPQ. Additional control reactions included tubulin incubated with Hrr25ΔPQ or K38AΔPQ in the absence of γTuSC-Spc110$^{1\text{-}401}$. The resulting microtubules were fixed, centrifuged onto coverslips, and visualized by immunofluorescence. Representative images are shown. Scale bar, 20 μm. (C) Microtubules assembled in the assays described in A were quantified. Microtubules in 10 fields were counted for each condition. The mean number of microtubules is shown for each condition (n = 4–7 for nucleation assays with no kinase or 12.5–100 nM kinase; n = 2 for control assays without γTuSC-Spc110$^{1\text{-}401}$). Error bars represent SEM. Two-tailed t tests suggest significant differences in nucleation activity between the γTuSC-Spc110$^{1\text{-}401}$ complex alone and γTuSC-Spc110$^{1\text{-}401}$ with Hrr25ΔPQ ($p \leq 0.15$, 12.5 nM; $p \leq 0.06$, 25 nM; $p \leq 0.04$, 50 nM; $p \leq 0.02$, 100 nM) or γTuSC-Spc110$^{1\text{-}401}$ with K38AΔPQ ($p \leq 0.0004$, 50 nM; $p \leq 0.02$, 100 nM).

We further demonstrated that inhibition of Hrr25 kinase activity results in abnormally long cytoplasmic microtubules. A similar phenotype was previously observed in *tub4* mutants (Marschall *et al.*, 1996), possibly because nuclear/spindle microtubule formation is inhibited, making more α/β-tubulin available for microtubule assembly in the cytoplasm. Alternatively, events at the SPB might affect stability of distant microtubule ends if SPBs serve as loading sites for microtubule stability–regulating factors (Cuschieri *et al.*, 2007). Our genetic data implicate Hrr25, like Tub4, in the Kar9 spindle-positioning pathway. Such a function might be a reflection of the long

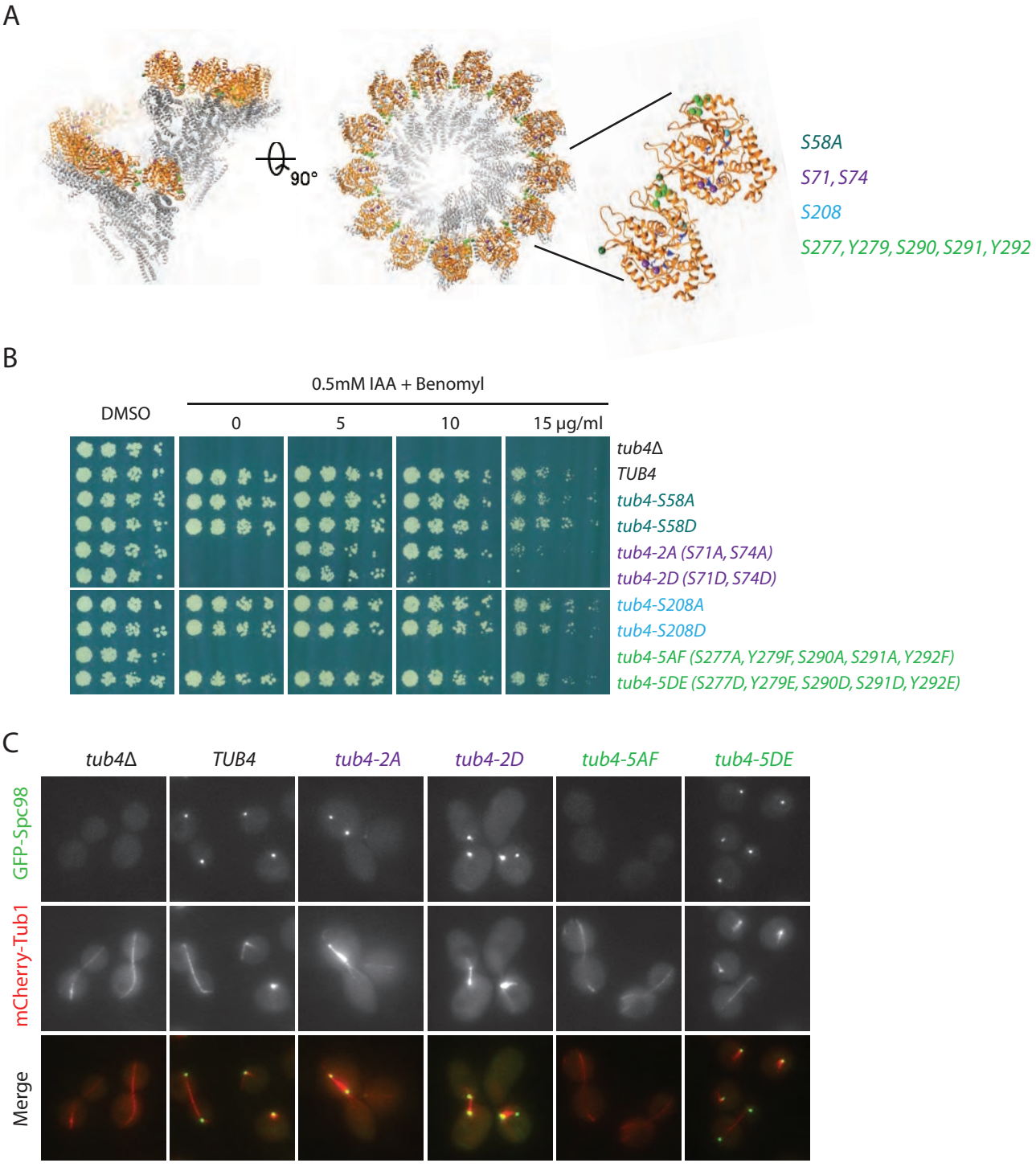

FIGURE 7: Mutation of Hrr25 phosphorylation sites on yeast γ-tubulin support a role in γTuSC regulation in vivo. (A) Side (left) and plus-end views (middle) of a pseudoatomic model of the yeast γ-tubulin ring complex with two enlarged, laterally interacting γ-tubulins (right; Kollman *et al.*, 2015). γ-Tubulins, orange; Spc97/98, gray; GTP-binding residues, navy. Hrr25 phosphorylation sites of interest are highlighted on the γ-tubulins: dark green (S58) indicates the Hrr25 phosphorylation site on the H1-S2 loop. Purple (S71 and S74) indicates the phosphorylation sites on the plus end of γ-tubulin, where it interacts with α-tubulin. Cyan (S208) indicates the phosphorylation site on helix 6. Green (S277, Y279, S290, S291, Y292) indicates phosphorylation sites that reside between γ-tubulin monomers. (B) *TUB4-AID* cells expressing *tub4*Δ, wild-type *TUB4*, or *tub4* phosphomutants were grown on YPD medium containing auxin (0.5 mM) or auxin with the indicated concentrations of benomyl at 25°C. (C) *TUB4-AID* cells expressing *tub4*Δ, wild-type *TUB4*, or *tub4* phosphomutants along with GFP-Spc98 and mCherry-Tub4 were treated with 0.5 mM auxin for 1 h at 25°C before imaging. Maximum intensity *Z*-projections of representative cells are presented. Scale bar, 2 µm.

cytoplasmic microtubules observed in mutants of both proteins. Alternatively, Hrr25 might directly phosphoregulate components of the Kar9 pathway in addition to components of the SPB.

We showed that Hrr25 directly phosphorylates γTuSC components in vivo and in vitro. Phenotypes of Tub4 phosphorylation-site mutants suggest that Hrr25 may regulate Tub4 functions through two distinct mechanisms. Phosphorylation at S71 and S74 may promote interaction of γ-tubulin with α/β-tubulin. In contrast, Tub4 phosphorylation at S277, Y279, S290, S291, and Y292, which are located at the γ-tubulin/γ-tubulin interface, may be critical for γTuSC and/or γTuRC complex integrity. Of greater importance, in both cases, mutation to alanine resulted in defects that implicate Hrr25 in a *positive* regulatory role, consistent with the fact that inhibition of Hrr25 kinase activity leads to microtubule defects. Previously two phosphorylation sites of Tub4 (S360, phosphorylated by Cdk1, and Y455, phosphorylated by an unknown kinase) were shown to be crucial for Tub4 function (Vogel *et al.*, 2001; Keck *et al.*, 2011; Lin *et al.*, 2011). Mutation of either site to acidic residues, but not to alanine, resulted in microtubule defects, suggesting that these phosphorylation sites might negatively regulate Tub4. We note discrepancies between phenotypes caused by Hrr25 loss of function and mutation of Hrr25's phosphorylation sites in Tub4. These differences might be accounted for by the fact that multiple protein kinases target γTuRC in vivo, and these kinases may have overlapping/partially redundant effects in cells. It is important to note that the Hrr25 phosphorylation sites that we mapped in Tub4 have not been validated as bona fide phosphorylation sites in vivo. Future work will be needed to address how phosphorylation by a group of protein kinases regulates Tub4.

Cryo-electron microscopic analysis of the budding yeast γTuRC structure suggested that the complex might be activated via a conformational change that results in an arrangement of γ-tubulins within the ring that precisely matches 13-protofilament microtubule architecture (Kollman *et al.*, 2010). Indeed, artificially capturing the "closed-ring" γTuRC state through mutagenesis enhances nucleation activity in vitro (Kollman *et al.*, 2015). It has been proposed that in vivo activation of γTuRC might be achieved allosterically through a regulatory protein binding to γTuRC and/or posttranslational modifications of γTuRC. In more complex eukaryotes, a centrosomal scaffold protein CDK5RAP2 targets γTuRC to centrosomes and the Golgi apparatus (Wang *et al.*, 2010) and stimulates nucleation activity of the complex in vitro (Choi *et al.*, 2010). However, the mechanism by which CDK5RAP2 activates γTuRC is unclear. In addition, a wide variety of kinases have been found to regulate γTuRC function (Luders *et al.*, 2006; Izumi *et al.*, 2008; Alvarado-Kristensson *et al.*, 2009; Haren *et al.*, 2009; Zhang *et al.*, 2009; Bahtz *et al.*, 2012; Sdelci *et al.*, 2012; Liu *et al.*, 2014). It was recently reported that NME7 localizes at the centrosome and that its kinase activity is required for efficient microtubule nucleation (Liu *et al.*, 2014). The studies reported here biochemically and genetically identified the yeast CK1δ protein Hrr25 as an interacting partner of γTuRC in vivo and implicate Hrr25 in γTuRC regulation.

It has long been known that CK1δ is enriched at centrosomes. However, evidence for microtubule-related functions has only been reported recently. CK1δ promotes centrosome translocation to the immunological synapse during T-cell activation, a process requiring remodeling of the microtubule network. CK1δ binds and phosphorylates the microtubule plus-end protein EB1, and disruption of CK1δ-EB1 interaction perturbs centrosome translocation (Zyss *et al.*, 2011). CK1δ is also crucial for neurite outgrowth via regulation of the Wnt-signaling pathway. Specifically, centrosomal localization of CK1δ is essential for its function in Wnt signaling (Greer and Rubin, 2011). Inhibition of CK1δ expression or kinase activity blocks ciliogenesis through multiple mechanisms, including CK1δ interaction with AKAP450 and microtubule nucleation at the Golgi (Greer *et al.*, 2014). It is known that AKAP450 recruits both CK1δ (Sillibourne *et al.*, 2002) and γTuRC (Takahashi *et al.*, 2002; Rivero *et al.*, 2009) to centrosomes. However, whether CK1δ directly regulates γTuRC remains unexplored. Because CK1δ and γTuRC are conserved in all eukaryotes, we expect that the mechanism by which Hrr25 regulates yeast γTuSC is shared in more complex organisms, including humans, in which CK1δ has been implicated a variety of diseases. At the same time, it will be important to identify all of the targets through which Hrr25 regulates the microtubule cytoskeleton.

MATERIALS AND METHODS

Yeast strains

The yeast strains used in this study are listed in Supplemental Table S3. Cells were grown in yeast extract/peptone/dextrose (YPD) or selective medium at 25°C unless otherwise specified.

Identification of Hrr25-associated proteins

Hrr25-TAP was purified from yeast cells expressing the tagged protein from the endogenous genomic locus as described (Cheeseman *et al.*, 2001), with the modification that 150 mM KCl was used throughout the purification.

Hrr25-TAP and associated proteins were incubated in digestion buffer (8 M urea, 100 mM Tris, pH 8.5). The mixture was brought to 5 mM Tris (2-carboxyethyl) phosphine and incubated at room temperature for 15 min. Iodoacetamide was then added to 10 mM and the resultant mixture incubated at room temperature for 20 min in dark. The samples were then diluted fourfold with 100 mM Tris (pH 8.5) and digested overnight with 1/40 enzyme/protein ratio of trypsin (Promega, Madison, WI) at 37°C.

Digested peptide mixtures were pressure loaded onto a Kasil-fritted fused silica capillary column (250-μm inner diameter [i.d.]) packed with 3 cm of 5-μm Partisphere strong cation exchange resins (SCX; Whatman, Clifton, NJ) and 3 cm of 5-μm Aqua C18 resins (RP; Phenomenex, Ventura, CA). The column was then washed with buffer containing 95% water, 5% acetonitrile, and 0.1% formic acid. After desalting, this sample-loaded back-end column was then connected to a 100-μm-i.d. capillary column with a 5-μm pulled tip packed with 10 cm of 3-μm Aqua C18 material through a zero-dead-volume union (Upchurch, Oak Harbor, WA), and the entire three-phase column was placed inline with an Agilent 1200 quaternary HPLC (Agilent, Palo Alto, CA), and a modified 9-step MudPIT analysis described previously (Washburn *et al.*, 2001) was performed. Three buffer solutions were used: 5% acetonitrile/0.1% formic acid (buffer A); 80% acetonitrile/0.1% formic acid (buffer B), and 500 mM ammonium acetate/5% acetonitrile/0.1% formic acid (buffer C). The first step consisted of a 60-min gradient from 0 to 100% buffer B. Steps 2–9 had the following gradient profile: 3 min of 100% buffer A, 5 min of *X*% buffer C (*X* = 10, 20, 30, 40, 50, 60, 80, and 100%, respectively, for the analysis of steps 2–9), a 10-min gradient from 0 to 10% buffer B, a 70-min gradient from 10 to 45% buffer B, a 10-min gradient from 45 to 100% buffer B, and a 10-min equilibration of 100% buffer A. As peptides were eluted from the microcapillary column, they were electrosprayed directly into an LTQ-Orbitrap mass spectrometer (Thermo Fisher Scientific, San Jose, CA) with the application of a distal 2.5-kV spray voltage. A cycle of one full-scan mass spectrum (400–1600 *m*/*z*, 60,000 resolution), followed by 10 data-dependent collision-induced dissociation tandem mass

spectrometry (MS/MS) spectra at a 35% normalized collision energy, was repeated continuously throughout each step of the multidimensional separation. Application of mass spectrometer scan functions and HPLC solvent gradients was controlled by the Xcalibur data system (Thermo Fisher Scientific).

MS/MS spectra were extracted using RawXtract (version 1.9.9; McDonald *et al.*, 2004) and searched with the ProLuCID algorithm (Xu *et al.*, 2006) against a *Saccharomyces cerevisiae* database concatenated to a decoy database in which the sequence for each entry in the original database was reversed. A static modification (+57.02146) on cysteine was added to the search. The precursor mass tolerance was set as 50 ppm, and fragment mass tolerance was set as 600 ppm. The enzyme specificity was semitryptic, with number of missed cleavages at 2. ProLuCID search results were assembled and filtered using the DTASelect, version 2.0, program (Cociorva *et al.*, 2007), requiring a minimum of two peptides per protein identification. The protein identification false-positive rate was held <1%, and all peptide-spectra matches were required to have <5 ppm mass error.

Live-cell imaging

Yeast strains were grown to log phase at 25°C in synthetic medium lacking tryptophan and then immobilized on concanavalin A–coated coverslips. All images of yeast cells were obtained using an Olympus (Tokyo, Japan) IX81 microscope equipped with a 100×/1.4 numerical aperture objective and an Orca-ER charge-coupled device camera (Hamamatsu, Hamamatsu, Japan).

Immuno–electron microscopy

Hrr25-3GFP was localized by immuno–electron microscopy as described previously (Giddings *et al.*, 2001). Briefly, specimens were prepared by cryofixation in a Wohlwend Compact 02 High Pressure Freezer, followed by freeze substitution in 0.25% glutaraldehyde/0.1% uranyl acetate in acetone at −80°C and embedding in Lowicryl HM20 resin. Serial 70-nm-thick sections were immunostained with an affinity-purified rabbit polyclonal anti-GFP primary antibody (a generous gift from Chad Pearson, University of Colorado, Denver, CO) diluted in 1% nonfat dry milk in phosphate-buffered saline/Tween 20 (0.1%) followed by goat-anti-rabbit 15-nm gold secondary antibody (Ted Pella, Reading, CA). Samples were imaged in a Philips CM100 transmission electron microscope (FEI, Hillsboro. OR).

Immunoblotting

Yeast total cell extracts were prepared from log-phase cells as previously described (Foiani *et al.*, 1994). Total cell extracts were subjected to immunoblot analysis. Proteins were detected using the following primary antibodies: mouse anti-Hrr25 (Abmart, Berkeley Heights, NJ), rabbit anti-GFP (Molecular Probes, Eugene, OR), mouse anti-V5 (Invitrogen, Carlsbad, CA), mouse anti-Pgk1 (Invitrogen). Blots were subsequently scanned using an Odyssey Infrared Imager (LI-COR Biosciences, Lincoln, NE).

Protein expression and purification

γTuSC- Spc110$^{1\text{-}401}$ was expressed and purified as described previously (Kollman *et al.*, 2010). Pig brain tubulin was purified according to Castoldi and Popov (2003). Hrr25-Strep-hexahistidine (6xHis) and Hrr25-K38A-Step-6xHis proteins were expressed in yeast and purified as described (Peng *et al.*, 2015). Hrr25ΔPQ-Strep-6xHis and Hrr25ΔPQ-K38A-Step-6xHis proteins were expressed in yeast and purified as the full-length proteins using lysis buffer (50 mM potassium phosphate, pH 8.0, 300 mM KCl, 10 mM imidazole, 1 mM dithiothreitol [DTT], 5 mM $MgCl_2$, 10% glycerol), wash buffer (50 mM potassium phosphate, pH 8.0, 300 mM KCl, 20 mM imidazole, 1 mM DTT, 5 mM $MgCl_2$, 10% glycerol), and elution buffer (50 mM potassium phosphate, pH 8.0, 300 mM KCl, 500 mM imidazole, 1 mM DTT, 5 mM $MgCl_2$, 10% glycerol).

In vitro kinase assays

In vitro phosphorylation was performed as described previously (Peng and Weisman, 2008).

Microtubule nucleation assays

Pure γTuSC-Spc110$^{1\text{-}401}$ (Kollman *et al.*, 2015), Hrr25ΔPQ, Hrr25ΔPQ-K38A, and pig brain tubulin were diluted at the appropriate concentrations into microtubule assembly buffer (80 mM K–1,4-piperazinediethanesulfonic acid [PIPES], pH 6.9, 100 mM KCl, 10% glycerol, 1 mM ethylene glycol tetraacetic acid [EGTA], 5 mM $MgCl_2$, 1 mM GTP, 1 mM ATP, 1 mM DTT) on ice. Reactions were incubated at 30°C for 20 min, fixed 3 min in 10 volumes of 1% glutaraldehyde in BRB80 (80 mM K-PIPES, pH 6.9, 1 mM EGTA, 1 mM $MgCl_2$), and then diluted 10 times into BRB80 (final volume, 1.5 ml). A 1-ml amount of the resulting fixed reactions was layered onto 20% glycerol/BRB80 cushions and centrifuged for 45 min, 24,000 × *g*, onto 18-mm-round coverslips. Microtubules were visualized on the coverslips by immunofluorescence with fluorescein isothiocyanate–conjugated mouse anti–α-tubulin (F2168; Sigma-Aldrich, St. Louis, MO).

ACKNOWLEDGMENTS

We thank Elmar Schiebel, Trisha Davis, Wolfgang Zachariae, Tim Stearns, and Doug Koshland for sharing reagents. We especially thank Thomas Eng and Vincent Guacci for their help with the auxin-inducible degron system and Charles Greenberg for sharing structural modeling data before publication. This work is supported by National Institutes of Health Grants RO1 GM47842 (G.B.), P41 RR011823 (J.Y.), RO1 GM031627 (D.A.A.), RO1 GM51312 (M.W.), and PO1 GM105537 (D.A.A., M.W.).

REFERENCES

Aldaz H, Rice LM, Stearns T, Agard DA (2005). Insights into microtubule nucleation from the crystal structure of human gamma-tubulin. Nature 435, 523–527.

Alvarado-Kristensson M, Rodriguez MJ, Silio V, Valpuesta JM, Carrera AC (2009). SADB phosphorylation of gamma-tubulin regulates centrosome duplication. Nat Cell Biol 11, 1081–1092.

Andersen JS, Wilkinson CJ, Mayor T, Mortensen P, Nigg EA, Mann M (2003). Proteomic characterization of the human centrosome by protein correlation profiling. Nature 426, 570–574.

Bahtz R, Seidler J, Arnold M, Haselmann-Weiss U, Antony C, Lehmann WD, Hoffmann I (2012). GCP6 is a substrate of Plk4 and required for centriole duplication. J Cell Sci 125, 486–496.

Behrend L, Stoter M, Kurth M, Rutter G, Heukeshoven J, Deppert W, Knippschild U (2000). Interaction of casein kinase 1 delta (CK1delta) with post-Golgi structures, microtubules and the spindle apparatus. Eur J Cell Biol 79, 240–251.

Castillo AR, Meehl JB, Morgan G, Schutz-Geschwender A, Winey M (2002). The yeast protein kinase Mps1p is required for assembly of the integral spindle pole body component Spc42p. J Cell Biol 156, 453–465.

Castoldi M, Popov AV (2003). Purification of brain tubulin through two cycles of polymerization-depolymerization in a high-molarity buffer. Protein Expr Purif 32, 83–88.

Cheeseman IM, Brew C, Wolyniak M, Desai A, Anderson S, Muster N, Yates JR, Huffaker TC, Drubin DG, Barnes G (2001). Implication of a novel multiprotein Dam1p complex in outer kinetochore function. J Cell Biol 155, 1137–1145.

Cheong JK, Virshup DM (2011). Casein kinase 1: complexity in the family. Int J Biochem Cell Biol 43, 465–469.

Choi YK, Liu P, Sze SK, Dai C, Qi RZ (2010). CDK5RAP2 stimulates microtubule nucleation by the gamma-tubulin ring complex. J Cell Biol 191, 1089–1095.
Cociorva D, Tabb DL, Yates JR (2007). Validation of tandem mass spectrometry database search results using DTASelect. Curr Protoc Bioinformatics Chapter 13, Unit 13.14.
Costanzo M, Baryshnikova A, Bellay J, Kim Y, Spear ED, Sevier CS, Ding H, Koh JL, Toufighi K, Mostafavi S, *et al*. (2010). The genetic landscape of a cell. Science 327, 425–431.
Crasta K, Lim HH, Giddings TH Jr, Winey M, Surana U (2008). Inactivation of Cdh1 by synergistic action of Cdk1 and polo kinase is necessary for proper assembly of the mitotic spindle. Nat Cell Biol 10, 665–675.
Cuschieri L, Miller R, Vogel J (2006). Gamma-tubulin is required for proper recruitment and assembly of Kar9-Bim1 complexes in budding yeast. Mol Biol Cell 17, 4420–4434.
Cuschieri L, Nguyen T, Vogel J (2007). Control at the cell center: the role of spindle poles in cytoskeletal organization and cell cycle regulation. Cell Cycle 6, 2788–2794.
Fasolo J, Sboner A, Sun MG, Yu H, Chen R, Sharon D, Kim PM, Gerstein M, Snyder M (2011). Diverse protein kinase interactions identified by protein microarrays reveal novel connections between cellular processes. Genes Dev 25, 767–778.
Foiani M, Marini F, Gamba D, Lucchini G, Plevani P (1994). The B subunit of the DNA polymerase alpha-primase complex in Saccharomyces cerevisiae executes an essential function at the initial stage of DNA replication. Mol Cell Biol 14, 923–933.
Friedman DB, Kern JW, Huneycutt BJ, Vinh DB, Crawford DK, Steiner E, Scheiltz D, Yates J 3rd, Resing KA, Ahn NG, Winey M, Davis TN (2001). Yeast Mps1p phosphorylates the spindle pole component Spc110p in the N-terminal domain. J Biol Chem 276, 17958–17967.
Friedman DB, Sundberg HA, Huang EY, Davis TN (1996). The 110-kD spindle pole body component of Saccharomyces cerevisiae is a phosphoprotein that is modified in a cell cycle-dependent manner. J Cell Biol 132, 903–914.
Giddings TH Jr, O'Toole ET, Morphew M, Mastronarde DN, McIntosh JR, Winey M (2001). Using rapid freeze and freeze-substitution for the preparation of yeast cells for electron microscopy and three-dimensional analysis. Methods Cell Biol 67, 27–42.
Gombos L, Neuner A, Berynskyy M, Fava LL, Wade RC, Sachse C, Schiebel E (2013). GTP regulates the microtubule nucleation activity of gamma-tubulin. Nat Cell Biol 15, 1317–1327.
Goshima G, Mayer M, Zhang N, Stuurman N, Vale RD (2008). Augmin: a protein complex required for centrosome-independent microtubule generation within the spindle. J Cell Biol 181, 421–429.
Greer YE, Rubin JS (2011). Casein kinase 1 delta functions at the centrosome to mediate Wnt-3a-dependent neurite outgrowth. J Cell Biol 192, 993–1004.
Greer YE, Westlake CJ, Gao B, Bharti K, Shiba Y, Xavier CP, Pazour GJ, Yang Y, Rubin JS (2014). Casein kinase 1delta functions at the centrosome and Golgi to promote ciliogenesis. Mol Biol Cell 25, 1629–1640.
Guillet V, Knibiehler M, Gregory-Pauron L, Remy MH, Chemin C, Raynaud-Messina B, Bon C, Kollman JM, Agard DA, Merdes A, Mourey L (2011). Crystal structure of gamma-tubulin complex protein GCP4 provides insight into microtubule nucleation. Nat Struct Mol Biol 18, 915–919.
Haren L, Stearns T, Luders J (2009). Plk1-dependent recruitment of gamma-tubulin complexes to mitotic centrosomes involves multiple PCM components. PLoS One 4, e5976.
Hoekstra MF, Dhillon N, Carmel G, DeMaggio AJ, Lindberg RA, Hunter T, Kuret J (1994). Budding and fission yeast casein kinase I isoforms have dual-specificity protein kinase activity. Mol Biol Cell 5, 877–886.
Hoekstra MF, Liskay RM, Ou AC, DeMaggio AJ, Burbee DG, Heffron F (1991). HRR25, a putative protein kinase from budding yeast: association with repair of damaged DNA. Science 253, 1031–1034.
Inclan YF, Nogales E (2001). Structural models for the self-assembly and microtubule interactions of gamma-, delta- and epsilon-tubulin. J Cell Sci 114, 413–422.
Izumi N, Fumoto K, Izumi S, Kikuchi A (2008). GSK-3beta regulates proper mitotic spindle formation in cooperation with a component of the gamma-tubulin ring complex, GCP5. J Biol Chem 283, 12981–12991.
Kafadar KA, Zhu H, Snyder M, Cyert MS (2003). Negative regulation of calcineurin signaling by Hrr25p, a yeast homolog of casein kinase I. Genes Dev 17, 2698–2708.
Keck JM, Jones MH, Wong CC, Binkley J, Chen D, Jaspersen SL, Holinger EP, Xu T, Niepel M, Rout MP, *et al.* (2011). A cell cycle phosphoproteome of the yeast centrosome. Science 332, 1557–1561.
Knippschild U, Gocht A, Wolff S, Huber N, Lohler J, Stoter M (2005a). The casein kinase 1 family: participation in multiple cellular processes in eukaryotes. Cell Signal 17, 675–689.
Knippschild U, Wolff S, Giamas G, Brockschmidt C, Wittau M, Wurl PU, Eismann T, Stoter M (2005b). The role of the casein kinase 1 (CK1) family in different signaling pathways linked to cancer development. Onkologie 28, 508–514.
Knop M, Schiebel E (1997). Spc98p and Spc97p of the yeast gamma-tubulin complex mediate binding to the spindle pole body via their interaction with Spc110p. EMBO J 16, 6985–6995.
Knop M, Schiebel E (1998). Receptors determine the cellular localization of a gamma-tubulin complex and thereby the site of microtubule formation. EMBO J 17, 3952–3967.
Kollman JM, Greenberg CH, Li S, Moritz M, Zelter A, Fong KK, Fernandez JJ, Sali A, Kilmartin J, Davis TN, Agard DA (2015). Ring closure activates yeast gammaTuRC for species-specific microtubule nucleation. Nat Struct Mol Biol 22, 132–137.
Kollman JM, Merdes A, Mourey L, Agard DA (2011). Microtubule nucleation by gamma-tubulin complexes. Nat Rev Mol Cell Biol 12, 709–721.
Kollman JM, Polka JK, Zelter A, Davis TN, Agard DA (2010). Microtubule nucleating gamma-TuSC assembles structures with 13-fold microtubule-like symmetry. Nature 466, 879–882.
Kollman JM, Zelter A, Muller EG, Fox B, Rice LM, Davis TN, Agard DA (2008). The structure of the gamma-tubulin small complex: implications of its architecture and flexibility for microtubule nucleation. Mol Biol Cell 19, 207–215.
Li YY, Yeh E, Hays T, Bloom K (1993). Disruption of mitotic spindle orientation in a yeast dynein mutant. Proc Natl Acad Sci USA 90, 10096–10100.
Lin TC, Gombos L, Neuner A, Sebastian D, Olsen JV, Hrle A, Benda C, Schiebel E (2011). Phosphorylation of the yeast gamma-tubulin Tub4 regulates microtubule function. PLoS One 6, e19700.
Lin TC, Neuner A, Schlosser YT, Scharf AN, Weber L, Schiebel E (2014). Cell-cycle dependent phosphorylation of yeast pericentrin regulates gamma-TuSC-mediated microtubule nucleation. Elife 3, e02208.
Liu P, Choi YK, Qi RZ (2014). NME7 is a functional component of the gamma-tubulin ring complex. Mol Biol Cell 25, 2017–2025.
Lord C, Bhandari D, Menon S, Ghassemian M, Nycz D, Hay J, Ghosh P, Ferro-Novick S (2011). Sequential interactions with Sec23 control the direction of vesicle traffic. Nature 473, 181–186.
Lowe J, Li H, Downing KH, Nogales E (2001). Refined structure of alpha beta-tubulin at 3.5 A resolution. J Mol Biol 313, 1045–1057.
Luders J, Patel UK, Stearns T (2006). GCP-WD is a gamma-tubulin targeting factor required for centrosomal and chromatin-mediated microtubule nucleation. Nat Cell Biol 8, 137–147.
Lusk CP, Waller DD, Makhnevych T, Dienemann A, Whiteway M, Thomas DY, Wozniak RW (2007). Nup53p is a target of two mitotic kinases, Cdk1p and Hrr25p. Traffic 8, 647–660.
Maekawa H, Usui T, Knop M, Schiebel E (2003). Yeast Cdk1 translocates to the plus end of cytoplasmic microtubules to regulate bud cortex interactions. EMBO J 22, 438–449.
Marschall LG, Jeng RL, Mulholland J, Stearns T (1996). Analysis of Tub4p, a yeast gamma-tubulin-like protein: implications for microtubule-organizing center function. J Cell Biol 134, 443–454.
McDonald WH, Tabb DL, Sadygov RG, MacCoss MJ, Venable J, Graumann J, Johnson JR, Cociorva D, Yates JR 3rd (2004). MS1, MS2, and SQT-three unified, compact, and easily parsed file formats for the storage of shotgun proteomic spectra and identifications. Rapid Commun Mass Spectrom 18, 2162–2168.
Michelot A, Costanzo M, Sarkeshik A, Boone C, Yates JR 3rd, Drubin DG (2010). Reconstitution and protein composition analysis of endocytic actin patches. Curr Biol 20, 1890–1899.
Miller RK, Matheos D, Rose MD (1999). The cortical localization of the microtubule orientation protein, Kar9p, is dependent upon actin and proteins required for polarization. J Cell Biol 144, 963–975.
Milne DM, Looby P, Meek DW (2001). Catalytic activity of protein kinase CK1 delta (casein kinase 1delta) is essential for its normal subcellular localization. Exp Cell Res 263, 43–54.
Murakami A, Kimura K, Nakano A (1999). The inactive form of a yeast casein kinase I suppresses the secretory defect of the sec12 mutant. Implication of negative regulation by the Hrr25 kinase in the vesicle budding from the endoplasmic reticulum. J Biol Chem 274, 3804–3810.
Nishimura K, Fukagawa T, Takisawa H, Kakimoto T, Kanemaki M (2009). An auxin-based degron system for the rapid depletion of proteins in nonplant cells. Nat Methods 6, 917–922.

Peng Y, Grassart A, Lu R, Wong CC, Yates J 3rd, Barnes G, Drubin DG (2015). Casein kinase 1 promotes initiation of clathrin-mediated endocytosis. Dev Cell 32, 231–240.
Peng Y, Weisman LS (2008). The cyclin-dependent kinase Cdk1 directly regulates vacuole inheritance. Dev Cell 15, 478–485.
Pereira G, Knop M, Schiebel E (1998). Spc98p directs the yeast gamma-tubulin complex into the nucleus and is subject to cell cycle-dependent phosphorylation on the nuclear side of the spindle pole body. Mol Biol Cell 9, 775–793.
Perez DI, Gil C, Martinez A (2011). Protein kinases CK1 and CK2 as new targets for neurodegenerative diseases. Med Res Rev 31, 924–954.
Petronczki M, Matos J, Mori S, Gregan J, Bogdanova A, Schwickart M, Mechtler K, Shirahige K, Zachariae W, Nasmyth K (2006). Monopolar attachment of sister kinetochores at meiosis I requires casein kinase 1. Cell 126, 1049–1064.
Pollard TD (2010). A guide to simple and informative binding assays. Mol Biol Cell 21, 4061–4067.
Ray P, Basu U, Ray A, Majumdar R, Deng H, Maitra U (2008). The Saccharomyces cerevisiae 60 S ribosome biogenesis factor Tif6p is regulated by Hrr25p-mediated phosphorylation. J Biol Chem 283, 9681–9691.
Remy MH, Merdes A, Gregory-Pauron L (2013). Assembly of gamma-tubulin ring complexes: implications for cell biology and disease. Prog Mol Biol Transl Sci 117, 511–530.
Rivero S, Cardenas J, Bornens M, Rios RM (2009). Microtubule nucleation at the cis-side of the Golgi apparatus requires AKAP450 and GM130. EMBO J 28, 1016–1028.
Schafer T, Maco B, Petfalski E, Tollervey D, Bottcher B, Aebi U, Hurt E (2006). Hrr25-dependent phosphorylation state regulates organization of the pre-40S subunit. Nature 441, 651–655.
Sdelci S, Schutz M, Pinyol R, Bertran MT, Regue L, Caelles C, Vernos I, Roig J (2012). Nek9 phosphorylation of NEDD1/GCP-WD contributes to Plk1 control of gamma-tubulin recruitment to the mitotic centrosome. Curr Biol 22, 1516–1523.
Sillibourne JE, Milne DM, Takahashi M, Ono Y, Meek DW (2002). Centrosomal anchoring of the protein kinase CK1delta mediated by attachment to the large, coiled-coil scaffolding protein CG-NAP/AKAP450. J Mol Biol 322, 785–797.
Song S, Grenfell TZ, Garfield S, Erikson RL, Lee KS (2000). Essential function of the polo box of Cdc5 in subcellular localization and induction of cytokinetic structures. Mol Cell Biol 20, 286–298.
Stirling DA, Stark MJ (1996). The phosphorylation state of the 110 kDa component of the yeast spindle pole body shows cell cycle dependent regulation. Biochem Biophys Res Commun 222, 236–242.
Stoter M, Bamberger AM, Aslan B, Kurth M, Speidel D, Loning T, Frank HG, Kaufmann P, Lohler J, Henne-Bruns D, *et al*. (2005). Inhibition of casein kinase I delta alters mitotic spindle formation and induces apoptosis in trophoblast cells. Oncogene 24, 7964–7975.
Takahashi M, Yamagiwa A, Nishimura T, Mukai H, Ono Y (2002). Centrosomal proteins CG-NAP and kendrin provide microtubule nucleation sites by anchoring gamma-tubulin ring complex. Mol Biol Cell 13, 3235–3245.
Teixido-Travesa N, Roig J, Luders J (2012). The where, when and how of microtubule nucleation—one ring to rule them all. J Cell Sci 125, 4445–4456.
Vogel J, Drapkin B, Oomen J, Beach D, Bloom K, Snyder M (2001). Phosphorylation of gamma-tubulin regulates microtubule organization in budding yeast. Dev Cell 1, 621–631.
Vogel J, Snyder M (2000). The carboxy terminus of Tub4p is required for gamma-tubulin function in budding yeast. J Cell Sci 113, 3871–3882.
Wang Z, Wu T, Shi L, Zhang L, Zheng W, Qu JY, Niu R, Qi RZ (2010). Conserved motif of CDK5RAP2 mediates its localization to centrosomes and the Golgi complex. J Biol Chem 285, 22658–22665.
Washburn MP, Wolters D, Yates JR 3rd (2001). Large-scale analysis of the yeast proteome by multidimensional protein identification technology. Nat Biotechnol 19, 242–247.
Xu T, Venable JD, Park SK, Cociorva D, Lu B, Liao L, Wohlschlegel J, Hewel J, Yates JR 3rd (2006). ProLuCID, a fast and sensitive tandem mass spectra-based protein identification program. Mol Cell Proteomics 5, S174.
Zhang X, Chen Q, Feng J, Hou J, Yang F, Liu J, Jiang Q, Zhang C (2009). Sequential phosphorylation of Nedd1 by Cdk1 and Plk1 is required for targeting of the gammaTuRC to the centrosome. J Cell Sci 122, 2240–2251.
Zyss D, Ebrahimi H, Gergely F (2011). Casein kinase I delta controls centrosome positioning during T cell activation. J Cell Biol 195, 781–797.